# Supporting Information for "Calving multiplier effect controlled by melt undercut geometry"

D. A. Slater[1,2], D. I. Benn[1], T. R. Cowton[1], J. N. Bassis[3] and J. A. Todd[1]

1. School of Geography and Sustainable Development, University of St Andrews

2. School of Geosciences, University of Edinburgh

3. Department of Space Sciences and Engineering, University of Michigan

# Contents of this file



# S1 Derivation of depth-integrated torque ($M$) and shear ($Q$) at the terminus

## S1.1 Depth-integrated torque

We here evaluate the depth-integrated torque integral $M = \int F \times r\, dr$ described in section 2.2 of the main article. $F$ is the force per unit width acting on the terminus due to ice or water pressure $p$. Using vector components and the linear undercut geometry shown in Fig. 1b of the main article, on the terminus above the water we have $F = [p, 0, 0]\, dz$, $r = [u, 0, z - H/2]$ and $F \times r = -p\,[0, z - H/2, 0]\, dz$. The angle of the calving front below the water, measured from the horizontal, is $\tan\theta = d/u$. Below the water, therefore, we have $F = p\,[1, 0, -1/\tan\theta]\, dz$, $r = [z/\tan\theta, 0, z - H/2]$ and $F \times r = -p\,[0, z/\sin^2\theta - H/2, 0]\, dz$. The pressure moment due to ice pressure $p_i = \rho_i g(H-z)$ both above and below the water is then

$$
\begin{aligned}
&-\rho_i g \int_d^H (H-z)\left(z-\frac{H}{2}\right)\,dz - \rho_i g \int_0^d (H-z)\left(\frac{z}{\sin^2\theta}-\frac{H}{2}\right)\,dz \\
&= \frac{1}{12}\rho_i g H^3 + \left(\frac{1}{3}\rho_i g d - \frac{1}{2}\rho_i g H\right)u^2
\end{aligned}
\tag{S1}
$$

The pressure moment due to water pressure $p_w = \rho_w g(H-z)$ is

$$
\begin{aligned}
&\rho_w g \int_0^d (d-z)\left(\frac{z}{\sin^2\theta}-\frac{H}{2}\right)\,dz \\
&= \frac{1}{6}\rho_w g d^3 + \frac{1}{6}\rho_w g d u^2 - \frac{1}{4}\rho_w g H d^2
\end{aligned}
\tag{S2}
$$

So that the overall moment for the linear undercut case is as in Eq. 9 of the main article, given by

$$
M = \frac{1}{12}\rho_i g H^3 + \frac{1}{6}\rho_w g d^3 - \frac{1}{4}\rho_w g H d^2 + \left(\frac{1}{3}\rho_i g d - \frac{1}{2}\rho_i g H + \frac{1}{6}\rho_w g d\right)u^2 \tag{S3}
$$

In the uniformly undercut case, the calving front has three parts: vertical under water, horizontal and vertical above water (Fig. 1c of the main article). Over the vertical under water part, $F = [p\,dz, 0, 0]$, $r = [0, 0, z-H/2]$ and $F \times r = [0, -p\,(z-H/2)\,dz, 0]$. The contribution to the moment is

$$
\begin{aligned}
&-\rho_i g \int_0^d (H-z)\left(z-\frac{H}{2}\right)\,dz + \rho_w g \int_0^d (d-z)\left(z-\frac{H}{2}\right)\,dz \\
&= -\rho_i g\left(-\frac{H^2 d}{2}-\frac{d^3}{3}+\frac{3Hd^2}{4}\right) + \rho_w g\left(\frac{d^3}{6}-\frac{Hd^2}{4}\right)
\end{aligned}
\tag{S4}
$$

Over the horizontal part, $F = [0, 0, -p]\,dx$, $r = [x, 0, d-H/2]$ and $F \times r = [0, -p\,x, 0]\,dx$. The contribution to the moment is

$$
-\rho_i g(H-d)\int_0^u x\,dx = -\rho_i g(H-d)\frac{u^2}{2} \tag{S5}
$$

Over the vertical above water part, $F = [p, 0, 0]\,dz$, $r = [u, 0, z-H/2]$ and $F \times r = [0, -p\,(z-$

$H/2)\, dz, 0]$. The contribution to the moment is

$$\begin{aligned} &-\rho_i g \int_d^H (H-z)\left(z-\frac{H}{2}\right)\, dz \\ &= \rho_i g \left(\frac{H^3}{12} - \frac{H^2 d}{2} - \frac{d^3}{3} + \frac{3Hd^2}{4}\right) \end{aligned} \tag{S6}$$

The total moment in the uniformly undercut case is then

$$M = \frac{1}{12}\rho_i g H^3 + \frac{1}{6}\rho_w g d^3 - \frac{1}{4}\rho_w g H d^2 - \frac{1}{2}\rho_i g (H-d) u^2 \tag{S7}$$

## S1.2 Depth-integrated shear

To derive the expression for the depth-mean shear stress over the undercut region, consider a block of linearly undercut ice with the left side of the block a distance $x$ from the grounding line and the right side at the calving front (Fig. 1b of the main article). Note $0 \leq x \leq u$. In the main article, only the case where the left hand side of the block is at the grounding line ($x = 0$) is considered, but here we retain the dependence on $x$ so that we can later show (section S2) that the depth-mean shear is almost always greatest at the grounding line. Over its length, the block has a mean thickness of

$$H - d + \frac{u-x}{2}\frac{d}{u} \tag{S8}$$

and, therefore, the weight of the block per unit width of glacier is

$$\rho_i g\,(u-x)\left(H - d + \frac{u-x}{2}\frac{d}{u}\right) \tag{S9}$$

The mean thickness of the submerged part of the block is

$$\frac{(u-x)d}{2u} \tag{S10}$$

and, therefore, the weight of water displaced by the block is

$$\rho_w g\,(u-x)\,\frac{(u-x)d}{2u} \tag{S11}$$

The depth-integrated shear stress within the ice at the left-hand side of the block can be expressed as the product of the depth-mean shear stress, $q$, and the ice thickness at that point

$$q\left[H - d + (u - x)\frac{d}{u}\right] \tag{S12}$$

Finally, the depth-integrated shear stress must compensate for the imbalance between the weight of the block of ice and the weight of the water it displaces, which after some rearrangement gives

$$q\left[H - d + (u - x)\frac{d}{u}\right] = \rho_i g\,(u - x)\left[H - d + \frac{u - x}{2}\frac{d}{u}\left(1 - \frac{\rho_w}{\rho_i}\right)\right] \tag{S13}$$

If the left hand side of the block is taken to be at the grounding line ($x = 0$), the left hand side of the equation is $Q$, and the right hand side of the equation simplifies to give Eq. 7 of the main article

$$Q = \rho_i g u H\left[1 - \frac{d}{2H}\left(1 + \frac{\rho_w}{\rho_i}\right)\right] \tag{S14}$$

The equivalent analysis for the uniformly undercut block (Fig. 1c of the main article) is more straightforward. The weight of the block as a function of $x$ is

$$\rho_i g\,(u - x)\,(H - d) \tag{S15}$$

and the block displaces no water. The thickness of the left-hand side of the block is $H - d$ and the depth-mean shear stress is then given by

$$(H - d)\,q = \rho_i g(u - x)\,(H - d) \tag{S16}$$

when the left hand side of the block is taken to be at the grounding line, the left hand side of the equation becomes $Q$ and the right hand side simplifies to give the expression in the main article

$$Q = \rho_i g u\,(H - d) \tag{S17}$$

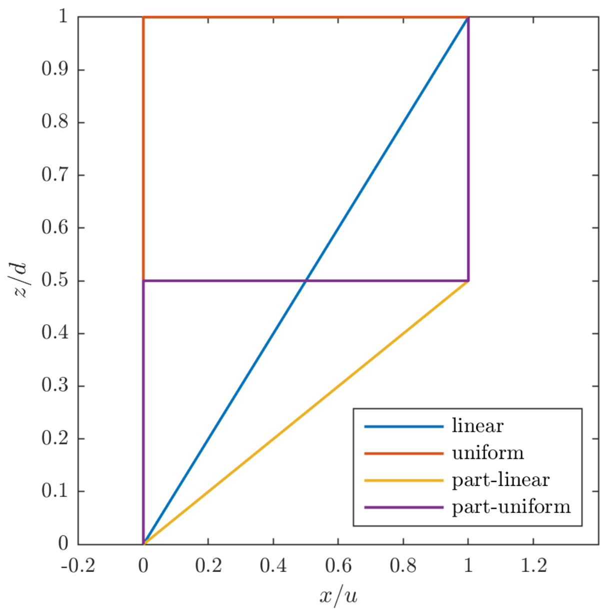


Figure S1: Various undercut shapes for which expressions for torque and shear are given. The part-linear and part-uniform shapes are plotted with a fraction $a = 1/2$.

### S1.3 Other calving front shapes

We here list the torque and shear expressions for the other undercut shapes shown in Fig. S1.

For part-linear undercutting extending to a fraction $a$ of the water depth (such that $a = 0$ is a vertical calving front and $a = 1$ is the linear undercutting considered in the main article) we have

$$M = \frac{1}{12}\rho_i g H^3 + \frac{1}{6}\rho_w g d^3 - \frac{1}{4}\rho_w g H d^2 + \left[\frac{1}{3}\rho_i g a d - \frac{1}{2}\rho_i g H + \frac{1}{6}\rho_w g d(3-2a)\right] u^2 \tag{S18}$$

$$Q = \rho_i g u H \left[1 - \frac{d}{2H}\left(a + \frac{\rho_w}{\rho_i}(2-a)\right)\right] \tag{S19}$$

For part-uniform undercutting extending to a fraction $a$ of the water depth (such that $a = 0$ is a vertical calving front and $a = 1$ is the uniform undercutting considered in the main article) we have

$$M = \frac{1}{12}\rho_i g H^3 + \frac{1}{6}\rho_w g d^3 - \frac{1}{4}\rho_w g H d^2 - \frac{1}{2}\rho_i g(H - ad)u^2 + \frac{1}{2}\rho_w g d(1-a)u^2 \tag{S20}$$

$$Q = \rho_i g u\,(H - ad) - \rho_w g u d\,(1-a) \tag{S21}$$

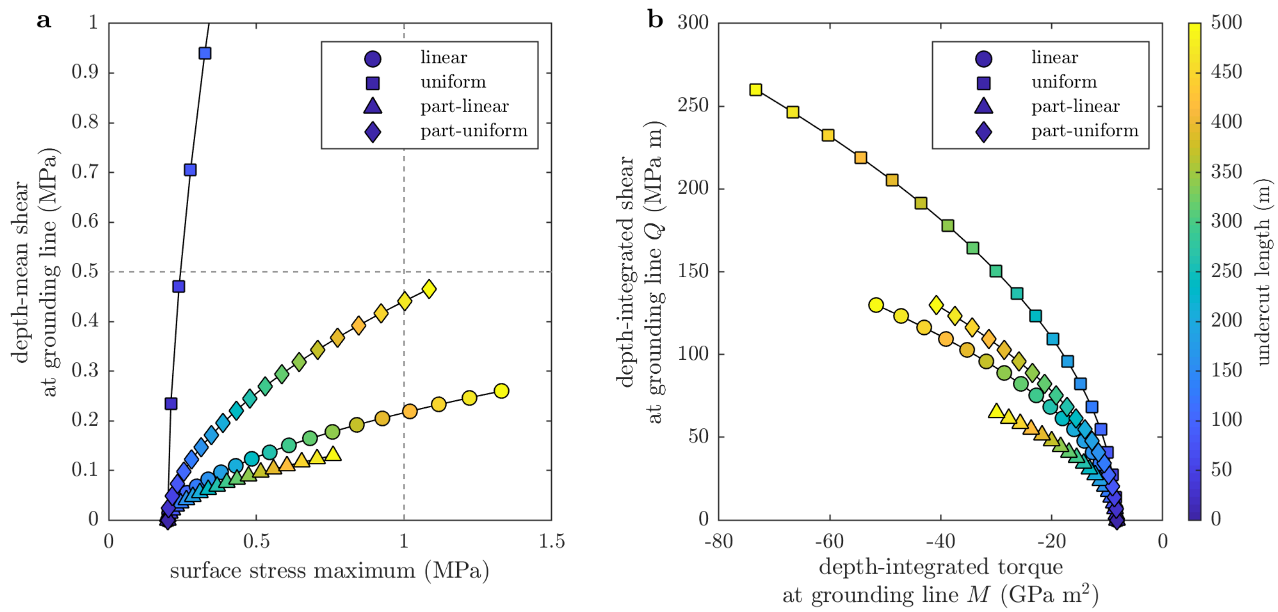


Figure S2: (a) Phase space plot of the surface tensile stress maximum versus the depth-mean shear stress at the grounding line as a function of undercut shape (marker style) and undercut length (marker colour). The calving thresholds of 1 MPa for tensile failure and 0.5 MPa for shear failure are shown as dashed grey lines. (b) The equivalent phase space plot of the depth-integrated torque $M$ versus the depth-integrated shear $Q$. All results assume an ice thickness of $H = 500$ m and a water depth such that the ice is at flotation. The part-linear and part-uniform results assume a shape fraction $a = 1/2$.

Fig. S2 shows the phase space for tensile versus depth-mean shear stress and depth-integrated torque versus depth-integrated shear as a function of undercut shape and length. It is seen that uniform undercutting extending over the full water depth is the shape most likely to undergo shear failure: as undercutting proceeds, the shear stress increases very quickly without a significant increase in the surface tensile stress (Fig. S2a). For linear and part-linear undercutting, the surface tensile stress increases quickly without significant increase in the shear stress, hence these undercut shapes promote rotational failure. Part-uniform undercutting lies in-between. Considering the depth-integrated quantities $M$ and $Q$ provides a similar picture (Fig. S2b), but it can be additionally noted that the depth-integrated quantities are less sensitive to the undercut shape, especially for little to moderate undercutting.

# S2 Depth-mean shear stress along the undercut

In the main article we consider only the depth-mean shear stress at the grounding line. Of course, it is possible that serac failure could occur at any point along the undercut, not just at the grounding line, particularly if the depth-mean shear stress is larger at that point than at the grounding line. For linear undercutting, the depth-mean shear stress at any point along the undercut, $q(x)$, is given by Eq. S13 and is plotted in Fig. S3a for various fractional water depths.

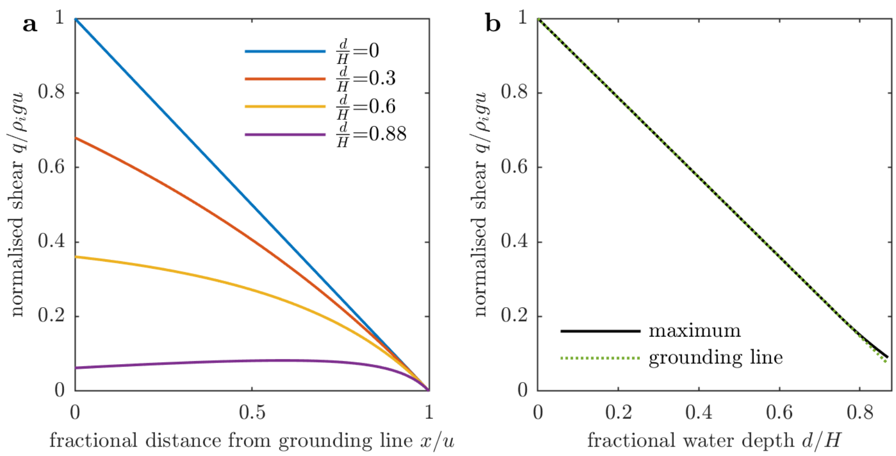


Figure S3: (a) Depth-mean shear as a function of fractional distance along the undercut for various fractional water depths from $d/H = 0$ (no water) to $d/H = 0.88$ (flotation). (b) Comparison of the maximum shear at any point along the undercut with the shear at the grounding line, both as a function of fractional water depth.

For all fractional water depths excepting those where the glacier is close to flotation, it is seen that the maximum depth-mean shear stress is located at the grounding line. When the fractional water depth is such that the glacier is close to flotation, the value of the shear stress at the grounding line remains a very good approximation of the maximum (Fig. S3b), but the location of the maximum is instead located at approximately three-quarters of the distance from the grounding line to the calving front (Fig. S3a). If serac failure were to occur at this position, it would change the undercut shape from linearly undercut, potentially influencing the next calving event. But, as is discussed in the main article, glaciers close to flotation undergoing linear undercutting are unlikely to experience serac failure (e.g. Fig. 9a of the main article) and so this difficulty can be avoided in the analysis, and it remains sufficient to assume that serac failure always occurs at the grounding line.

For uniform undercutting, it is easily seen from Eq. S16 that the depth-mean shear stress has its maximum at the grounding line. Thus, for both linear and uniform undercutting, only the shear at the grounding line is considered in the main article.

## S3 An alternative failure mechanism for uniform undercutting: cantilever failure

For uniform undercutting, the overhanging ice beyond the grounding line essentially forms a cantilever beam (Fig. 1c of the main article). In the main article we have considered how this may calve at the grounding line due to high shear stress, but an alternative failure mechanism is calving due to high tensile stress associated with the downward bending of this cantilever beam. Referring to this failure mechanism as 'cantilever' failure, it may be analysed by solving Eq. 1 of the main article for a beam of thickness $H - d$ and that is not in contact with the bed (so that $k = 0$). The resulting deflection of the beam from $w = 0$ at the grounding line is

$$w(x) = -\frac{(1-\nu^2)\rho_i g}{2E(H-d)^2}(6u^2x^2 - 4ux^3 + x^4) \tag{S22}$$

and the tensile stress on the beam surface is

$$\sigma_c(x) = \frac{3\rho_i g}{H-d}(u-x)^2 \tag{S23}$$

The maximum of the tensile stress is, therefore, at the grounding line ($x = 0$) with magnitude

$$\sigma_c = \frac{3\rho_i g u^2}{H-d} \tag{S24}$$

and the critical undercut length at which cantilever failure occurs is

$$u_c = \sqrt{\frac{H-d}{3\rho_i g}\sigma_r^{max}} \tag{S25}$$

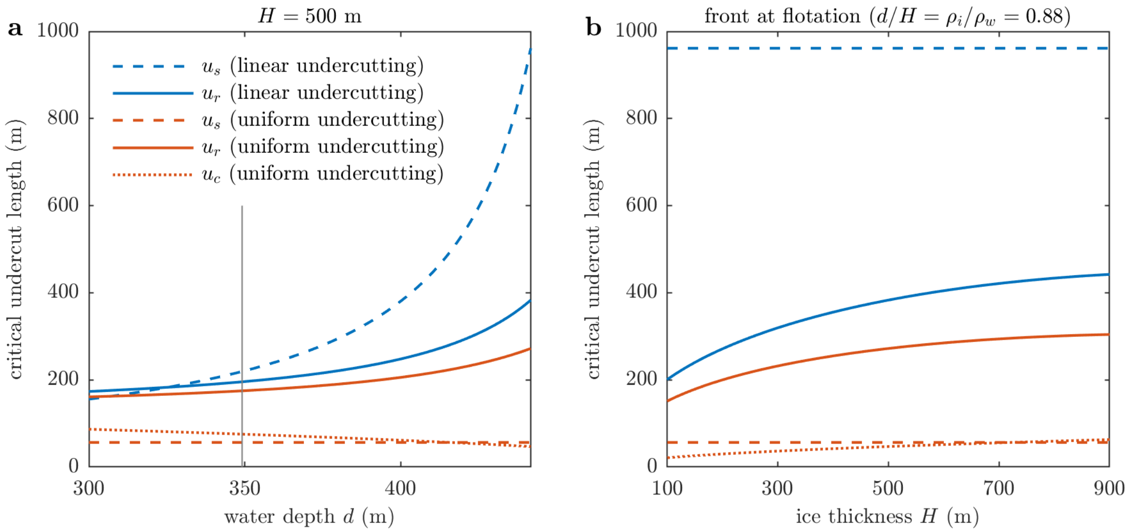


Figure S4: The same as Fig. 8 of the main article, but with the addition of the 'cantilever' failure length $u_c$ for uniform undercutting.

where $\sigma_r^{max} = 1$ MPa, as in the main article. For uniform undercutting, $u_c$ is plotted on Fig. S4. It is seen that the cantilever failure undercut length is very similar to the shear failure undercut length for uniform undercutting. Since both mechanisms imply failure at the same position (i.e. the grounding line), distinguishing between these mechanisms does not affect the main conclusions of the article. Extending this cantilever analysis to the linear undercut case is not straightforward because the large gradient of the ice thickness over the length of the cantilever makes it inappropriate to apply thin beam theory.

## S4 Basal longitudinal stress associated with bending

Similarly to Eq. 3 of the main article, the basal longitudinal stress associated with bending of the glacier is given by

$$\sigma_r = \frac{6D}{H^2} w'' = -\frac{6}{H^2} \left[ (M - Q\lambda) \sin\left(\frac{x}{\lambda}\right) - M \cos\left(\frac{x}{\lambda}\right) \right] \exp\left(\frac{x}{\lambda}\right) \tag{S26}$$

This basal longitudinal stress will be most positive when the terminus wants to rotate bottom-forwards into the ocean, and this tendency is maximised when $M$ is as large as possible (e.g. Fig. 3 of the main article and surrounding discussion) and when $Q$ is as small as possible (although we do not consider the case $Q < 0$). To maximise $M$ and minimise $Q$ we set $u = 0$ and $d = 0$ (i.e no undercutting and no water), which gives

$$\sigma_r = \frac{\rho_i g H}{2}\left[\cos\left(\frac{x}{\lambda}\right) - \sin\left(\frac{x}{\lambda}\right)\right]\exp\left(\frac{x}{\lambda}\right) \tag{S27}$$

Now for $x < 0$, we have $\exp\left(\frac{x}{\lambda}\right) < 1$ and $\cos\left(\frac{x}{\lambda}\right) - \sin\left(\frac{x}{\lambda}\right) < 2$, so that the basal longitudinal stress is at most $\rho_i g H$. The total stress, accounting for the basal stress resulting from bending and the cryostatic pressure (also $\rho_i g H$), is therefore smaller than 0 and is always compressive for the situations considered in this study.

# S5 Sensitivity to surface stress threshold

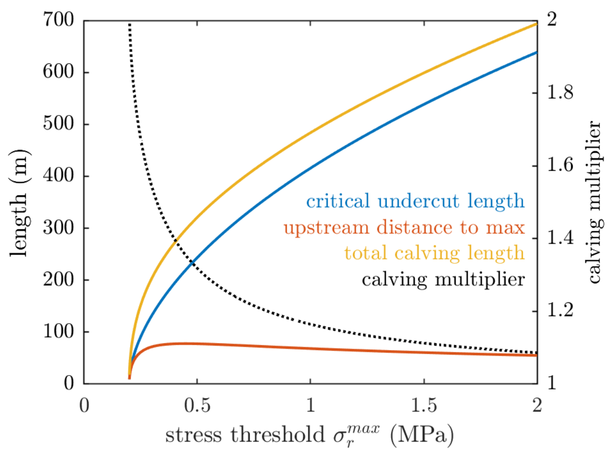


Figure S5: The sensitivity of the critical length scales for rotational calving and the calving multiplier to varying surface stress threshold. Results assume linear undercutting and a glacier of thickness 500 m at flotation.

The sensitivity of the critical length scales for rotational calving and the calving multiplier to varying surface stress threshold is shown in Fig. S5. The critical lengths for rotational failure are not defined for $\sigma_r^{max} < 0.2$ MPa because even a vertical calving front induces longitudinal stress at the glacier surface that exceeds this threshold. Above 0.2 MPa, the critical undercut length increases with the stress threshold because greater undercutting is required to generate sufficient stress at the glacier surface. In the main article we argued that the surface stress $\sigma_r$ scales approximately as $u^2/H$, and hence under variation in the surface stress threshold we would expect the critical undercut length to scale approximately as $(\sigma_r^{max})^{1/2}$, as seen in Fig. S5. In contrast, the upstream distance to the stress maximum is controlled largely by the characteristic length $\lambda$ (e.g. Eq. 5 and Fig. 10b of the main article), itself a function of the bed and ice strength and the ice thickness. The upstream distance to the stress maximum is, therefore, relatively insensitive to the stress threshold (Fig. S5). Lastly, since the calving multiplier is the ratio of the total calving length to the undercut length, the calving multiplier decreases with increasing surface stress threshold, with the approximate scaling $\beta \sim (\sigma_r^{max})^{-1/2}$.

While the values adopted for parameters in this study are within the ranges used by previous studies, these parameters are also rather idealised notions that assume the ice and bed are perfect and uniform. In reality, the ice will have crevasses and smaller imperfections and inhomogeneities and may display some viscous deformation. The bed will not be uniform and flat and subglacial water may influence the ice-bed contact. As a result, in a real-world application of our results, such as to form a calving parameterisation, a pragmatic choice would be to choose the values of these parameters to best match observations.